

Design principles for shift current photovoltaics

Ashley M. Cook*,^{1,2} Benjamin M. Fregoso*,¹ Fernando de Juan,¹ and Joel E. Moore^{1,3}

¹*Department of Physics, University of California, Berkeley, California, 94720, USA*

²*Department of Physics, University of Toronto, CAN*

³*Materials Sciences Division, Lawrence Berkeley National Laboratory, Berkeley, CA 94720*

While the basic principles and limitations of conventional solar cells are well understood, relatively little attention has gone toward evaluating and maximizing the potential efficiency of photovoltaic devices based on shift currents. In this work, a sum rule approach is introduced and used to outline design principles for optimizing shift currents for photon energies near the band gap, which depend on Berry connections as well as standard band structure. Using these we identify two new classes of shift current photovoltaics, ferroelectric polymer films and orthorhombic monochalcogenides, both of which exhibit peak photoresponsivities larger than predictions for previously known photovoltaics of this type. Using physically motivated tight-binding models, the full frequency dependent response of these materials is obtained. Exploring the phase space of these models, we find photoresponsivities that can exceed 100 mA/W. These results show that considering the microscopic origin of shift current via effective models allows one to improve the possible efficiency of devices using this mechanism and better grasp their potential to compete with conventional solar cells.

PACS numbers: 73.20.At,73.30.+y,71.20.-b,77.90.+k,73.50.-h, 73.61.-r

Introduction - Cost-effective, high-performing solar cell technology is an essential piece of a sustainable energy strategy. Exploring approaches to photo-current generation beyond conventional solar cells based on p-n junctions is worthwhile given that their performance is ultimately constrained by the Shockley-Queisser limit¹. One of the most promising alternative sources of photocurrent is the bulk photovoltaic effect (BPVE) or “shift current” effect, a non-linear optical response that yields net photocurrent in materials with net polarization²⁻¹⁰: the BPVE is able to generate an above band-gap photovoltage¹¹, potentially enabling solar cells based on the BPVE to surpass the Shockley-Queisser limit¹². Furthermore, there is evidence that the hybrid perovskite solar cells¹³⁻²⁶, an extremely active field of research and promising class of materials for photovoltaics, rely on this effect²⁷.

Despite considerable study of the BPVE a few decades ago, investigations into its optimization are much more recent. At present, it is clear a band gap in the visible spectrum (1.1-3.1 eV) is desirable for these kinds of solar cells^{28,29}. Maximizing the density of electronic transitions over the visible spectrum is also beneficial^{30,31}. Additionally, there is evidence that the shift current depends on the nature of electronic wavefunctions^{12,31}. Also, although net polarization in materials is necessary to achieve net shift current, shift current magnitude is not simply correlated with the magnitude of material polarization²⁹.

While these observations from studies of specific materials are important, better understanding of where to search for strong BPVE is desirable. To address this, we present simple design principles for BPVE optimization based on effective models, a proven approach in study of other complex materials phenomena such as thermoelectricity³²⁻³⁴. Our main design principle may be summarized as follows: the ideal BPVE device should have

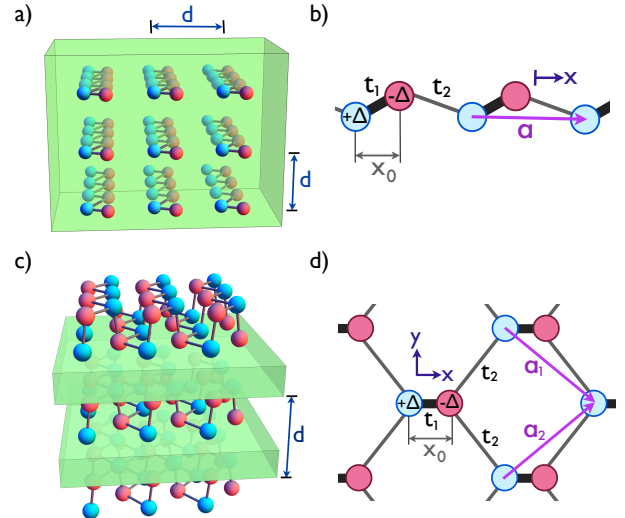


FIG. 1. a) 3D structure of a solar cell built by stacking one-dimensional ferroelectric polymers. b) Simplified two-band tight binding model of a polymer. c) 3D structure of a solar cell made by stacking two-dimensional monolayers of a monochalcogenide. The inert spacers between layers prevent the restoration of bulk inversion symmetry. d) Simplified two-band tight-binding model for a monochalcogenide layer.

a sharply rising peak in the response at the band edge, which should be closely aligned with the maximum of the solar spectrum (~ 1.5 eV). To understand how to maximize this peak, we present an effective model for the band edge for which the shift current can be expressed analytically in terms of the joint density of states and a simple prefactor. The simplicity of the expressions allows us to easily search for materials that maximize the prefactor.

Since the band edge always induces a Van Hove singularity in the density of states, the requirement of a large peak in any optical response can be naturally bet-

ter satisfied by low-dimensional materials, which generically present stronger singularities³⁵. Materials of one and two dimensions are therefore the focus of this work. Among one-dimensional materials, ferroelectric polymers are suitable candidates for shift-current photovoltaics: first, they break inversion symmetry as required by the BPVE, with in some cases suitable band gaps for photovoltaics applications^{36–39}. Second, ferroelectric polymers can be macroscopically oriented to generate large polarizations. For these reasons, we consider solar cells consisting of such polymer films, shown in Fig. 1(a). Two-dimensional materials⁴⁰ have great potential for photovoltaics, as shown by demonstration of a tunable photovoltaic effect (of the traditional p-n junction type) in graphene/dichalcogenide heterostructures^{41,42}, and in few-layer black phosphorus⁴³. Inspired by this work, we show here that a family of closely related materials, group IV monochalcogenides such as GeS^{44–47}, are able to realize high values of the BPVE. They are shown in the proposed heterostructure device in Fig.1(c).

Shift current - With electric field $E_b(\omega)$ at frequency ω and linearly-polarized in the b direction, the shift current is a DC response of the form⁶

$$J_a = \sigma^{abb}(\omega) E_b(\omega) E_b(-\omega). \quad (1)$$

Defining an intensity for each polarization, $I_{0,b} = c\epsilon_0 |E_b|^2/2$, we define the photoresponsivity κ^{abb} as the current density generated per incident intensity $J_a = \kappa^{abb} I_{0,b}$, where $\kappa^{abb} = 2\sigma^{abb}/c\epsilon_0$. For a D-dimensional system, κ^{abb} takes the form

$$\kappa^{abb} = C \int \frac{dk^D}{(2\pi)^D} \sum_{n,m} f_{nm} I_{nm}^{abb} \delta(\omega_{nm} - \omega), \quad (2)$$

where $C = 4g_s\pi e^3/\hbar^2\epsilon_0 c$, with c the speed of light, ϵ_0 the vacuum permittivity, and $g_s = 2$ accounts for the spin degeneracy. The sum is over all Bloch bands, with $\omega_{nm} = E_n - E_m$ the energy difference between bands n and m and $f_{nm} = f_n - f_m$ the difference of Fermi occupations, which we take at zero temperature. The integrand is

$$I_{nm}^{abb} = \text{Im}(r_{mn}^b r_{nm;a}^b), \quad (3)$$

where $r_{nm}^a = i \langle n | \partial_{k_a} m \rangle$, ($n \neq m$) are the inter-band matrix elements of the position operator (or inter-band Berry connections). A semicolon denotes a generalized derivative $r_{nm;a}^b = \partial_{k_a} r_{nm}^b - i(\xi_{nn}^a - \xi_{mm}^a) r_{nm}^b$, where $\xi_{nn}^a = i \langle n | \partial_{k_a} n \rangle$ is the diagonal Berry connection for band n .

Generic two band model - With the aim of describing the shift current response of the band edge of a semiconductor, next we consider the shift current of a generic two band model of the form

$$H = \epsilon_0 \sigma_0 + \vec{\sigma} \cdot \vec{f}, \quad (4)$$

where σ_0 is the identity matrix, $\vec{\sigma} = (\sigma_x, \sigma_y, \sigma_z)$ are the Pauli matrices and ϵ_0 and $\vec{f} = (f_x, f_y, f_z)$ are generic

functions of momenta \mathbf{k} (the momentum label is omitted to simplify notation). The conduction and valence bands are given by $E_1 = \epsilon_0 + \epsilon$, $E_2 = \epsilon_0 - \epsilon$, respectively and $\epsilon = (\vec{f} \cdot \vec{f})^{1/2}$.

To compute the shift current, the direct use of Eq. 3 requires the evaluation of derivatives of Bloch functions, which can be difficult numerically. An alternative way employs a sum rule to express Eq. 3 only in terms of matrix elements of the velocity operator^{4,9}, but this sum rule relies on the fact that in the plane wave basis $p = mv$, which is not applicable in the tight binding formalism. In this work we derived a novel sum rule appropriate for tight binding models (see Methods section), from which the integrand Eq. 3 can be evaluated for any two-band model

$$I_{12}^{abb} = - \sum_{ijm} \frac{1}{4\epsilon^3} (f_m f_{i,b} f_{j,ab} - f_m f_{i,b} f_{j,a} \frac{\epsilon_{,b}}{\epsilon}) \epsilon_{ijm}, \quad (5)$$

where the compact derivative notation $f_{i,a} \equiv \partial_{k_a} f_i$ is used. Since this expression does not depend on ϵ_0 , we set it to zero from now on.

This model can now be used to obtain the responsivity close to a band edge. To this end, we consider a direct band gap at a time reversal invariant momentum and expand the Hamiltonian around it

$$H = (\delta + \alpha_x k_x^2 + \alpha_y k_y^2 + \alpha_{xy} k_x k_y) \sigma_x + v_F k_x \sigma_y + (\Delta + \beta_x k_x^2 + \beta_y k_y^2 + \beta_{xy} k_x k_y) \sigma_z, \quad (6)$$

where we have set $\hbar = 1$. Time reversal symmetry $H^*(-\mathbf{k}) = H(\mathbf{k})$ prevents quadratic terms in σ_y , and we have taken the linear term to be in the x direction without loss of generality. The band gap of this model is $E_g = 2\epsilon|_{\mathbf{k}=0}$. From Eq. 5 we can evaluate the integrand to lowest order, which has the simple form

$$I_{12}^{xxx}(\omega) = \frac{4v_F}{\omega^3} (\alpha_x \Delta - \beta_x \delta) + O(\mathbf{k}^2), \quad (7)$$

$$I_{12}^{xyy}(\omega) = \frac{2v_F}{\omega^3} (\alpha_{xy} \Delta - \beta_{xy} \delta) + O(\mathbf{k}^2), \quad (8)$$

while $I_{12}^{yxx} = I_{12}^{yyy} = 0 + O(k^2)$. Note that in order to have a non-zero shift current quadratic terms in σ_x or σ_z are required. In 2D, the fact that I^{yxx} is in general non-zero means that the current need not be in the direction of the electric field polarization.

The shift current close to the band edge can now be obtained by substituting into Eq. 2, which gives

$$\kappa^{abb}(\omega) = C I_{12}^{abb}(\omega) N(\omega), \quad (\omega - E_g)/E_g \ll 1 \quad (9)$$

where $N(\omega) = \int dk^D \delta(\omega_{12} - \omega)/(2\pi)^D$ is the Joint Density of States (JDOS). This is one of the main results of this work. For ω close to the band edge, this simple expression allows one to optimize the effect by considering the contributions of the shift current integrand and the JDOS independently.

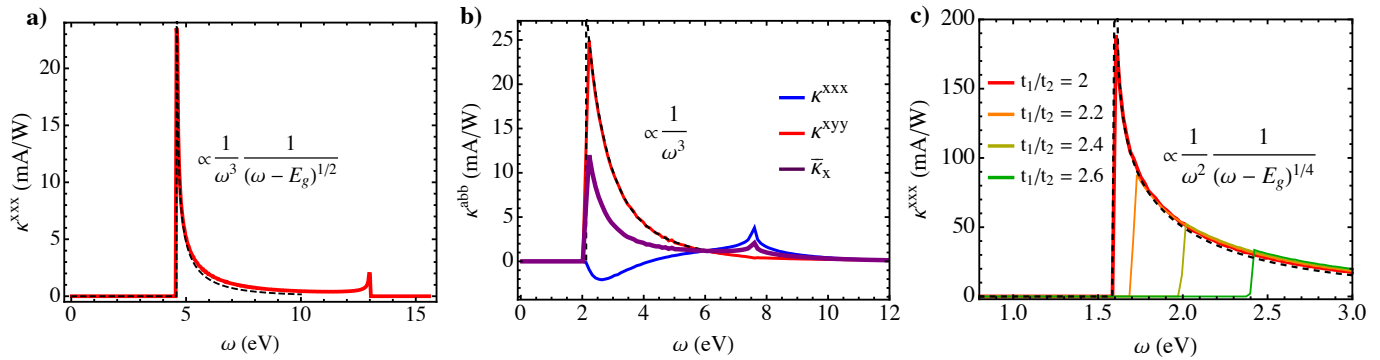


FIG. 2. Frequency dependence of the components of photoresponsivity κ^{abb} . (a) 1D model corresponding to the disubstituted polyacetylene, showing the square root divergence of the current at the band edges. (b) Various non-zero components of shift current tensor for a tight binding model of mono-chalcogenides. A large peak is observed in κ^{xxx} at the band edge. (c) Responsivity for $\Delta = 0.8$ and different hopping ratios approaching the semi-Dirac limit. The emergence of a singularity is observed. In the three figures, a dashed line shows the prediction of the effective low energy model valid near the edge, Eq. 9

A first simple strategy to maximize the response is therefore to look for band structures where the JDOS has a strong singularity. It is well known that in the 1D case, the generic JDOS diverges as a square root, $N(\omega) \propto (\omega - E_g)^{-1/2}$. 1D systems such as polymers or nanowires or systems in the quasi 1D limit will in general have a large response. In 2D, the band edge JDOS has a finite jump of $N(\omega) = (m_x m_y)^{1/2} / 2\pi$, where m_i are the average effective masses for valence and conduction bands. A singular $N(\omega)$ thus occurs in 2D when the inverse effective mass vanishes. In the effective model in Eq. 6, this happens when $\delta = 0$, which realizes what we may call a gapped semi-Dirac dispersion⁴⁸, since the coefficients of σ_y and σ_x are linear and quadratic in momentum, respectively. In such a case we have $N(\omega) \propto (\omega - E_g)^{-1/4}$ (full expressions for $N(\omega)$ may be found in the Methods section).

For materials with large JDOS, the current can be further enhanced by appropriately tuning the parameters in Eqs. 7-8. This is most easily discussed if these parameters can be related to microscopic lattice models. In the next section, we discuss tight-binding models for simple materials that realize the described types of band structures.

Material realizations and lattice models - To realize the 1D case, we consider ferroelectric polymers that break inversion symmetry such as Polyvinylidene Fluoride or Disubstituted Polyacetylene (DP)^{38,39,49}. This system is described by the tight-binding model schematically shown in Fig. 1(b). For a chain along the x-axis, the Hamiltonian is given by $f_x + if_y = -[t_1 e^{ik_x x_0} + t_2 e^{-ik_x(a-x_0)}]$ and $f_z = \Delta$. There are two types of hoppings, t_1 and t_2 , and alternating sites have different on-site potentials $\pm\Delta$. The lattice constant is a , and the sites within the unit cell are separated by a distance x_0 . Note that the dispersion does not depend on x_0 . Using Eq. 2 and Eq. 5 we can now compute the shift current for

this 1D model. Expanding about the low energy momentum $k_x = \pi/a$ and performing a constant rotation of the Pauli matrices, we obtain an effective model as Eq. 6 with parameters $k_y = 0$ and $\delta = t_1 - t_2$, $v_F = (t_1 - t_2)x_0 + t_2 a$, $\alpha_x = [t_2(a - x_0)^2 - t_1 x_0^2] / 2$.

To be able to compare the responsivity of these materials to that of a 3D system, we consider a stack of polymers as depicted in Fig. 1(a), separated by a distance d which we take to be equal to the lattice constant of the polymer $d = a$. The photoresponsivity is then $\kappa_{3D}^{abb} = \kappa_{1D}^{abb} / d^2$. The typical photoresponsivity spectrum of this model with this convention is shown in Fig. 2(a).

For the 2D case, we require a layered material that breaks both inversion and rotational symmetries. The most popular of the recently isolated 2D semiconductors break either inversion (BN, MoS₂) or rotational symmetries (black phosphorus⁵⁰, ReS₂⁵¹), but not both. An inversion symmetry breaking version of the strongly anisotropic black phosphorus, a group V element, can be obtained combining elements of the IV and VI groups. These group IV monochalcogenides, such as GeS, are predicted to be stable in the monolayer form with the orthorhombic structure of black phosphorus^{44,45}.

These materials can be described with a two band tight binding model, similar to the one used for black phosphorus^{52,53}. While in the actual structure the positions of Ge and S are at different heights and the unit cell contains four sites, for the purpose of this work we may consider a flattened structure where Ge and S form a distorted honeycomb lattice, as is done for black phosphorus⁵⁴. The Hamiltonian is $f_x + if_y = -e^{-ix_0 \mathbf{k}} [-t_1 + t_2 (e^{ia_1 \mathbf{k}} + e^{ia_2 \mathbf{k}})]$, where $\mathbf{x}_0 = (x_0, 0)$, and t_1 and t_2 are both positive^{52,53}. Again note the dispersion is independent of x_0 . The only difference with black phosphorus is that the on-site energies of the two elements are different, so $f_z = \Delta$. See Fig. 1(d) for definition of tight-binding model.

The effective model close to the band edge can be ob-

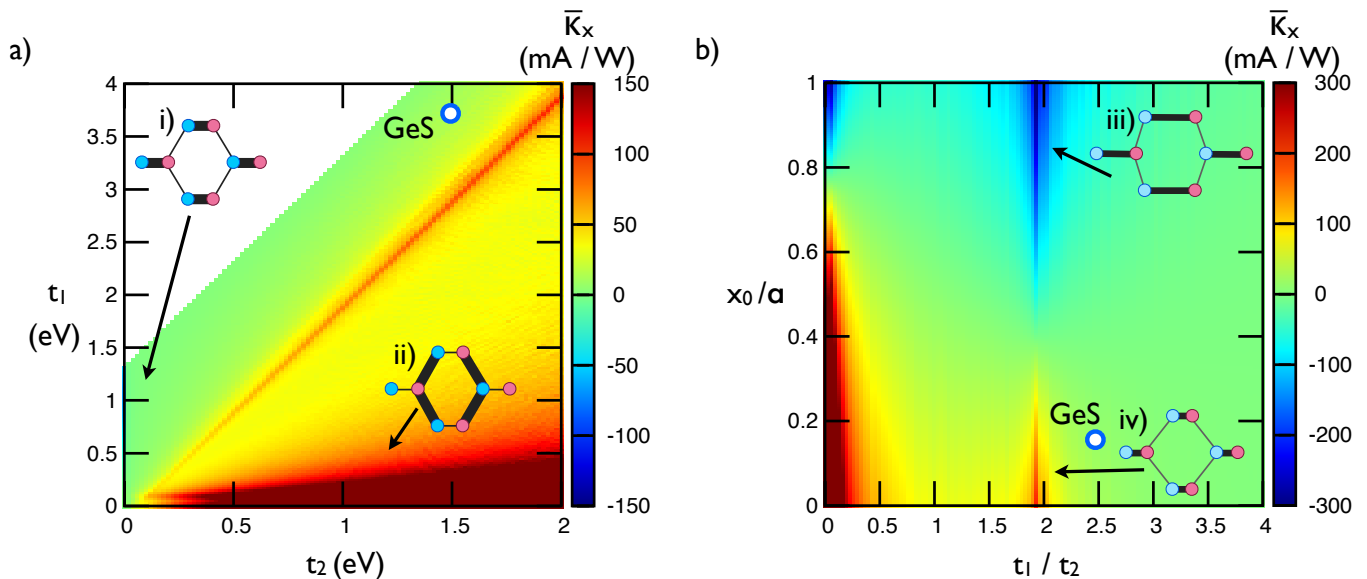


FIG. 3. (a) Polarization-averaged photoresponsivity in the x -direction, $\bar{\kappa}_x$, at the band gap frequency plotted as a function of hopping parameters t_1 and t_2 . Here, the band gap is held fixed at 2.6 eV and lattice distortion parameter $x_0 = 0.18a$, corresponding to the effective two-band model of GeS. (The location of GeS on the phase diagram is marked by a white circle with blue outline.) A white pixel value corresponds to a parameter set that could not yield the desired band gap. (i) and (ii) show bond strengths in the limits where $t_1 \gg t_2$ and $t_1 \ll t_2$, respectively, to illustrate the two extremes of the phase diagram. (b) Polarization-averaged photoresponsivity in the x -direction, $\bar{\kappa}_x$, at the band gap frequency plotted as a function of bond length x_0 (in units of lattice constant a) and ratio of hopping parameters t_1/t_2 . Here, Δ and t_2 are set to GeS values of 1.1 eV and 1.5 eV, respectively. The location of GeS on the phase diagram is marked by a white circle with blue outline. (iii) and (iv) show two extreme cases of the phase diagram, where x_0 is large and small, respectively.

tained by expanding around the Γ point, yielding $\delta = t_1 - 2t_2$, $v_F = t_1x_0 + 2t_2(a_x - x_0)$, $\alpha_x = [t_2(a_x - x_0)^2 - t_1x_0^2/2]$, $\alpha_y = t_2a_y^2$. In this lattice structure there is a mirror symmetry $y \rightarrow -y$, which is represented as the identity, and restricts $\alpha_{xy} = \beta_{xy} = 0$. In this model, the semi-Dirac case is realized when $t_1 = 2t_2$ ⁵⁵. We expect the monochalcogenides to have hoppings that satisfy $t_1 > 2t_2$ in general.

We consider a stack of monolayers separated by $d = a$, as shown in Fig. 1(c). In this case, we consider an inert spacer layer between the GeS layers to avoid the restoration of inversion symmetry that would occur if we were to stack GeS into its natural bulk form. The 3D photoresponsivity of this model, given by $\kappa_{3D}^{abb} = \kappa_{2D}^{abb}/d$, is shown in Fig. 2(b). We see that both κ^{xxx} and κ^{xyy} are in general finite, and the polarization average is also finite due to the strong anisotropy.

The response of the monochalcogenides is large because they are close in parameter space to the gapped semi-Dirac Hamiltonian. This is best illustrated by considering the evolution of a fictitious system where the hoppings are tuned from the physical parameters of GeS to the semi-Dirac case $t_1/t_2 = 2$, where the divergence of the response is clearly appreciated. This evolution is shown in Fig. 2(c).

Further optimization - After describing the representative tight-binding models with large JDOS, we may

now address a more systematic analysis of the photoresponsivity. First, we consider exploring the phase diagram of the monochalcogenides by sweeping t_1, t_2 in parameter space while the band gap is fixed at 2.6 eV by choosing Δ appropriately. Fig. 3(a) shows the polarization averaged photoresponsivity, $\bar{\kappa}_x = (\kappa^{xxx} + \kappa^{xyy})/2$, for the parameters $x_0 = 0.18a$ and $\theta = 0.69$. This phase diagram summarizes nicely the most physically relevant regimes where the shift current is large due to a divergent JDOS, namely the 1D dimensional limit where $t_1 \ll t_2$, and the semi-Dirac regime where $t_1 \sim 2t_2$. In this phase diagram, GeS is shown as a white circle with blue outline.

Next we illustrate a very important feature of the behavior of the shift current integrand. Eqs. 7-8 depend generically on the hoppings and lattice parameters. The energy does not depend on the parameter x_0 , but the wavefunctions do. In Fig. 3(b), we show the peak photoresponsivity as a function of t_1/t_2 and x_0 . A large response is observed in the semi-Dirac limit $t_1/t_2 \sim 2$. However, a very strong dependence on x_0 and even a sign change is also observed. The dependence on x_0 dramatically illustrates the fact that the shift current depends not only on the band structure, but also on the wavefunctions. This can be seen explicitly in the fact that the effective mass $m_x^{-1} = 4a_x^2t_1t_2/E_g$ is independent of x_0 , but the combination $v_F\alpha_x$ appearing in the shift current integrand is not. In particular α_x vanishes

for $x_0 = a_x/[1 + (|t_1/2t_2|)^{1/2}]$, which means that regardless of the JDOS, the band edge response can actually be zero. This behavior is characteristic of Berry connections, which depend explicitly on the positions of the sites in the unit cell.

Discussion - In this work, we have provided principles for designing materials with large shift current responses. We have done so by studying effective tight binding models for the band edge, which enables us to separate the JDOS contribution from the shift current integrand itself.

Several general conclusions can be drawn from the form of the effective shift current integrand in Eqs. 7-8. First, since the $1/\omega^3$ factor becomes $1/E_g^3$ at the band edge, materials with smaller gaps are expected to have larger shift currents. A second conclusion is that while looking for materials with large JDOS is a good guiding principle, the shift current integrand depends on other microscopic details that can change the response dramatically. Within our simple model, the shift current can be maximized by bringing the two sites of the unit cell closer together, which is a requirement that the monochalcogenides satisfy well.

Our results were made possible by the derivation of a new sum rule appropriate for tight-binding models. With this sum rule, our work can be easily extended to tight-binding models with more than two bands, or systems where the minimum direct gap is not at a time-reversal invariant momentum. We expect that the formalism developed here will provide the necessary link to combine ab-initio methods with effective models, allowing for more in-depth, systematic study of shift current photovoltaics.

Our results should be compared to known ferroelectric materials that have been recently studied. In the relevant range of energies for sunlight, $\omega \leq 4$ eV, we find peak values of 0.1 mA/W in BiFeO₃²⁸, 1 mA/W in hybrid perovskites²⁷ and a maximum 10-15 mA/W in BaTiO₃³⁰ or NaAsSe₂²⁹. For the realistic materials we propose, the peak response can reach twice that value, and with the additional advantage that the peak is by construction at the band edge. Moreover, as Fig. Fig. 2(c) and Fig. 3(b) show, peak responses on the order of several hundreds of mA/W could be achieved with materials closer to the semi-Dirac regime. To compare with conventional photovoltaic mechanisms, the total current per intensity of a crystalline Si solar cell exposed to sunlight is about 400 mA/W⁵⁶.

Given these numbers, our work is a tantalizing sign that shift current photovoltaics capable of surpassing conventional solar cells may be close at hand, and a push to investigate their full potential using a combination of these novel and also established techniques is warranted. We believe that the simple principles derived in our work will serve as a guide for both theory and experiment in the development and optimization of the next generation of shift current photovoltaics.

Methods

Shift current - To make contact with previous work,

we note the shift current integrand in Eq. 3 is sometimes expressed in terms of the phase of the inter-band matrix element $r_{nm}^b = |r_{nm}^b|e^{i\phi_{nm}^b}$ as $I_{nm}^{abb} = |r_{nm}^b|^2 R_{nm}^{a,b}$ where

$$R_{nm}^{a,b} = \partial_{k_a} \phi_{nm}^b - \xi_{na}^b + \xi_{nm}^a \quad (10)$$

is known as the shift vector.

The response to a natural light source such as sunlight, which is unpolarized, is obtained by averaging κ^{abb} over polarization. Taking $\vec{E}(\theta) = |E|(\cos \theta, \sin \theta)$ we have

$$\bar{J}_a = \int \frac{d\theta}{2\pi} J_a = \frac{1}{2}(\kappa^{aax} + \kappa^{aay})I_0 = \bar{\kappa}_a I_0 \quad (11)$$

Sum rule - The expression for the shift current presented in the main text can be obtained by the use of a sum rule for the quantity $r_{nm;b}^a$, which is obtained from the identity

$$\partial_{k_b} \partial_{k_a} \langle n|H|m \rangle = \delta_{nm} \partial_{k_b} \partial_{k_a} E_n. \quad (12)$$

Evaluating both sides explicitly for $n \neq m$, the identity can be expressed as

$$r_{nm;b}^a = -\frac{1}{i\omega_{nm}} \left[\frac{v_{nm}^a \Delta_{nm}^b + v_{nm}^b \Delta_{nm}^a}{\omega_{nm}} - w_{nm}^{ab} + \sum_{p \neq n,m} \left(\frac{v_{np}^a v_{pm}^b}{\omega_{pm}} - \frac{v_{np}^b v_{pm}^a}{\omega_{np}} \right) \right] \quad n \neq m \quad (13)$$

where $v_{nm}^b = \langle n|\partial_{k_b} H|m \rangle$ are the velocity matrix elements, $\Delta_{nm}^b = v_{nn}^b - v_{mm}^b$, $w_{nm}^{ba} = \langle n|\partial_{k_b} \partial_{k_a} H|m \rangle$ and $\omega_{nm} = E_n - E_m$. In the evaluation, we used

$$(r_{mn}^a)^* = r_{nm}^a \quad (14)$$

$$v_{nn}^a = \partial_{k_a} E_n \quad (15)$$

$$v_{nm}^a = i r_{nm}^a \omega_{nm} \quad n \neq m \quad (16)$$

The first equality follows from $\partial_{k_a} \langle n|m \rangle = 0$ if $m \neq n$, while the last two follow from $\partial_{k_a} \langle n|H|m \rangle = \delta_{nm} \partial_{k_a} E_n$. Note this sum rule contains the extra term w_{nm}^{ab} compared to Ref.⁹, where $H = p^2/2m + V(x)$ and $w_{nm}^{ab} = \delta_{nm} \delta^{ab}/m$ which has no off diagonal component.

Two band model - For the case of two bands, $m = 1, n = 2$ the use of the sum rule for the shift current integrand in Eq. 3 leads to the simplified expression

$$I_{nm}^{abb} = \frac{1}{\omega_{12}^2} \text{Im} \left[\frac{-v_{21}^b v_{12}^a (v_{11}^b - v_{22}^b)}{2\epsilon} + v_{21}^b w_{12}^{ba} \right] \quad (17)$$

To evaluate this expression we compute the wave functions of H

$$\psi_n = \frac{1}{\sqrt{2\epsilon}} (-\eta \sqrt{\epsilon - \eta f_z}, e^{i\phi_k} \sqrt{\epsilon + \eta f_z}) \quad (18)$$

with $n = 1, 2$, $\eta = (-1)^n$, and $\phi_k = \arctan(f_y/f_x)$. The required matrix elements are

$$v_{21}^a = \langle \psi_2 | (\epsilon_{0,a} \mathcal{I} + \sigma_i f_{i,a}) | \psi_1 \rangle = f_{i,a} s_i^* \quad (19)$$

$$v_{12}^{ab} = \langle \psi_1 | (\epsilon_{0,ab} \mathcal{I} + \sigma_i f_{i,ab}) | \psi_2 \rangle = f_{i,ab} s_i \quad (20)$$

where the off diagonal matrix element $s_i = \langle \psi_1 | \sigma_i | \psi_2 \rangle$ is

$$s_i = \left(\frac{f_x}{\epsilon} \cos \phi_k + i \sin \phi_k, \frac{f_x}{\epsilon} \sin \phi_k - i \cos \phi_k, -\frac{(f_x^2 + f_y^2)^{1/2}}{\epsilon} \right)$$

and the diagonal velocity matrix elements are computed from Eq. 15. The imaginary part in Eq. 17 can be taken using $\text{Im}[s_i^* s_j] = -\epsilon_{ijm} f_m / \epsilon$ and this leads to Eq. 5 in the main text.

Joint density of states To compute the Joint Density of states, we first start with the 1D case. Close to the band edge, we expand the energies of conduction and valence bands as $E_i \approx E_i(0) + k_x^2 / 2m_{i,x}$, so that $\omega_{12} = E_1 - E_2 \approx E_g + k_x^2 / 2m_x$ where the total effective mass $m_x^{-1} = |m_{1,x}|^{-1} + |m_{2,x}|^{-1}$ is given by

$$m_x^{-1} = 4(v_F^2 + 2\alpha_x \delta + 2\beta_x \Delta) / E_g \quad (21)$$

and solve for $k(\omega) = \sqrt{2m_x(\omega - E_g)}$. Rescaling $2m_x$ we get

$$\begin{aligned} N^{1D}(\omega) &= \sqrt{2m_x} \int \frac{dk \delta(k \pm k(\omega))}{2\pi |2k|} \\ &= \frac{\sqrt{2m_x}}{2\pi} \frac{\theta(\omega - E_g)}{\sqrt{(\omega - E_g)}} \end{aligned} \quad (22)$$

where we get the expected 1D singularity.

For the generic 2D case, again we expand $\omega_{12} \approx E_g + k_x^2 / 2m_x + k_y^2 / 2m_y$, where m_x is still given by Eq. 21 and

$$m_y^{-1} = 8(\alpha_y \delta + \beta_y \Delta) / E_g \quad (23)$$

We consider the case when $m_x > 0$, $m_y > 0$, so that the minimum does lie at $\vec{k} = 0$. By rescaling $2m_x$ and $2m_y$ we get in polar coordinates

$$\begin{aligned} N^{2D} &= \sqrt{4m_x m_y} \int \frac{k dk d\theta \delta(k - k(\omega))}{(2\pi)^2 |2k|} \\ &= \frac{\sqrt{m_x m_y}}{2\pi} \theta(\omega - E_g) \end{aligned} \quad (24)$$

which is the expected constant result. Finally, the semi-Dirac case occurs in 2D when $m_y^{-1} = 0$, which in the absence of second neighbor hopping occurs exactly at $\delta = 0$. In this case, we keep the complete expression for $\omega_{12} = ((\alpha_x k_x^2 + \alpha_y k_y^2)^2 + v_F^2 k_x^2 + \Delta^2)^{1/2}$. In polar coordinates we have

$$N^{SD} = \int \frac{k dk d\theta \delta(k - k(\omega))}{(2\pi)^2 |\partial_k \omega_{12}|} \quad (25)$$

We now rescale α_x, α_y instead, solve for k

$k(\omega) = [-v_F^2 / \alpha_x \cos^2 \theta \pm (v_F^4 / \alpha_x^2 \cos^4 \theta + \omega^2 - E_g^2)^{1/2}] / 2$ and get

$$\begin{aligned} N^{SD} &= \frac{\omega}{4\sqrt{\alpha_x \alpha_y}} \int \frac{dk d\theta \delta(k - k(\omega))}{(2\pi)^2 (v_F^4 / \alpha_x^2 \cos^4 \theta + \omega^2 - E_g^2)^{1/2}} \\ &= \frac{\Gamma(\frac{1}{4})}{4\Gamma(\frac{3}{4})(2\pi)^{3/2} |\alpha_x| \sqrt{\alpha_y} v_F} \frac{\omega \theta(\omega - E_g)}{(\omega^2 - E_g^2)^{1/4}} \end{aligned} \quad (26)$$

Material parameters An example of a disubstituted polyacetylene was experimentally realized in Ref. 38, with a band gap of 2.5 eV. For regular polyacetylene, where $\Delta = 0$, the hopping parameters and band gap have been estimated as⁴⁹ $t_1 = 2.85$ eV, $t_2 = 2.15$ eV, $E_g = 1.4$ eV. Assuming the same hopping for the disubstituted version, we require $\Delta = 1.0$ to match the observed band gap. The smallest neighbor distance after dimerization is⁴⁹ $x_0 = 0.48a$ with $a = 10\text{\AA}$.

For the monochalcogenide materials, in the absence of explicit tight binding models^{44,45}, we may use the parameters of monolayer black phosphorus as guidance^{52,53}. Indeed, one may check that beyond the structural similarity of these materials, their band structures and orbital content are also quite similar^{44,45,52,53}. We therefore follow Ref. 53 and, for GeS, take $t_1 = 3.7$ eV, $t_2 = 1.5$ eV, and fit $\Delta = 1.1$ eV to reproduce the direct gap at Γ of $E_g = 2.6$ eV. Note in Ref. 53 t_1 is actually negative, and we have accounted for this by an extra minus sign in the Hamiltonian for simplicity.

Acknowledgments - We thank J. Sipe, E. J. Mele, M. Bernardi, S. Coh, P. Král and F. Duque-Gomez for useful discussions. A.M.C was supported by the NSERC CGS-MSFSS and the NSERC CGS-D3, B.M.F was partially supported by Conacyt and NSF DMR-12065135, F. de Juan was supported by the U.S. Department of Energy, Office of Science, Basic Energy Sciences, Materials Sciences and Engineering Division, grant DE-AC02-05CH11231, and J.E.M. was supported by AFOSR MURI.

Author contributions - A.M.C. and B.M.F contributed equally to this work.

¹ W. Shockley and H. J. Queisser, J. Appl. Phys. **32**, 510 (1961).

² W. Kraut and R. von Baltz, Phys. Rev. B **19**, 1548 (1979).

³ V. I. Belinicher and B. I. Sturman, Soviet Physics Uspekhi **23**, 199 (1980).

⁴ R. von Baltz and W. Kraut, Phys. Rev. B **23**, 5590 (1981).

⁵ H. Presting and R. Von Baltz, physica status solidi (b)

112, 559 (1982).

⁶ B. I. Sturman and P. J. Sturman, *Photovoltaic and Photo-refractive Effects in Noncentrosymmetric Materials* (CRC Press, 1992).

⁷ C. Aversa and J. E. Sipe, Phys. Rev. B **52**, 14636 (1995).

⁸ N. Kristoffel, R. von Baltz, and D. Hornung, Zeitschrift für Physik B Condensed Matter **47**, 293 (1982).

- ⁹ J. E. Sipe and A. I. Shkrebtii, *Phys. Rev. B* **61**, 5337 (2000).
- ¹⁰ P. Král, E. J. Mele, and D. Tománek, *Phys. Rev. Lett.* **85**, 1512 (2000).
- ¹¹ W. Ji, K. Yao, and Y. C. Liang, *Advanced Materials* **22**, 1763 (2010).
- ¹² F. Wang and A. M. Rappe, *Phys. Rev. B* **91**, 165124 (2015).
- ¹³ G. Hodes, *Science* **342**, 317 (2013).
- ¹⁴ D. A. Egger, E. Edri, D. Cahen, and G. Hodes, *The Journal of Physical Chemistry Letters* **6**, 279 (2015), <http://dx.doi.org/10.1021/jz502726b>.
- ¹⁵ M. D. McGehee, *Nat Mater* **13**, 845 (2014).
- ¹⁶ M. Antonietta Loi and J. C. Hummelen, *Nat Mater* **12**, 1087 (2013).
- ¹⁷ J. Even, L. Pedesseau, J.-M. Jancu, and C. Katan, *The Journal of Physical Chemistry Letters* **4**, 2999 (2013), <http://dx.doi.org/10.1021/jz401532q>.
- ¹⁸ A. Stroppa, D. Di Sante, P. Barone, M. Bokdam, G. Kresse, C. Franchini, M.-H. Whangbo, and S. Picozzi, *Nat Commun* **5** (2014).
- ¹⁹ C. Zhang, D. Sun, C.-X. Sheng, Y. X. Zhai, K. Mielczarek, A. Zakhidov, and Z. V. Vardeny, *Nat Phys* **11**, 427 (2015).
- ²⁰ M. Saba, M. Cadelano, D. Marongiu, F. Chen, V. Sarritzu, N. Sestu, C. Figus, M. Aresti, R. Piras, A. Geddo Lehmann, C. Cannas, A. Musinu, F. Quochi, A. Mura, and G. Bongiovanni, *Nat Commun* **5** (2014).
- ²¹ A. M. A. Leguy, J. M. Frost, A. P. McMahon, V. G. Sakai, W. Kockelmann, C. Law, X. Li, F. Foglia, A. Walsh, B. C. O'Regan, J. Nelson, J. T. Cabral, and P. R. F. Barnes, *Nat Commun* **6** (2015).
- ²² C. Motta, F. El-Mellouhi, S. Kais, N. Tabet, F. Alharbi, and S. Sanvito, *Nat Commun* **6** (2015).
- ²³ M. R. Filip, G. E. Eperon, H. J. Snaith, and F. Giustino, *Nat Commun* **5** (2014).
- ²⁴ M. I. Saidaminov, A. L. Abdelhady, B. Murali, E. Alarousu, V. M. Burlakov, W. Peng, I. Dursun, L. Wang, Y. He, G. Maculan, A. Goriely, T. Wu, O. F. Mohammed, and O. M. Bakr, *Nat Commun* **6** (2015).
- ²⁵ C. Eames, J. M. Frost, P. R. F. Barnes, B. C. O'Regan, A. Walsh, and M. S. Islam, *Nat Commun* **6** (2015).
- ²⁶ J. H. Heo, S. H. Im, J. H. Noh, T. N. Mandal, C.-S. Lim, J. A. Chang, Y. H. Lee, H.-j. Kim, A. Sarkar, N. K., M. Gratzel, and S. I. Seok, *Nat Photon* **7**, 486 (2013).
- ²⁷ F. Zheng, H. Takenaka, F. Wang, N. Z. Koocher, and A. M. Rappe, *The Journal of Physical Chemistry Letters* **6**, 31 (2015).
- ²⁸ S. M. Young, F. Zheng, and A. M. Rappe, *Phys. Rev. Lett.* **109**, 236601 (2012).
- ²⁹ J. A. Brehm, S. M. Young, F. Zheng, and A. M. Rappe, *The Journal of chemical physics* **141**, 204704 (2014).
- ³⁰ S. M. Young and A. M. Rappe, *Phys. Rev. Lett.* **109**, 116601 (2012).
- ³¹ F. Wang, S. M. Young, F. Zheng, I. Grinberg, and A. M. Rappe, *ArXiv e-prints* (2015), [arXiv:1503.00679](https://arxiv.org/abs/1503.00679) [cond-mat.mtrl-sci].
- ³² G. Mahan and J. Sofo, *Proc. Natl. Acad. Sci. USA* **93**, 7436 (1996).
- ³³ F. J. DiSalvo, *Science* **285**, 703 (1999).
- ³⁴ P. Murphy, S. Mukerjee, and J. Moore, *Phys. Rev. B* **78**, 161406 (2008).
- ³⁵ L. Van Hove, *Phys. Rev.* **89**, 1189 (1953).
- ³⁶ H. S. Nalwa, ed., *Ferroelectric Polymers: Chemistry, Physics, and Applications* (CRC Press, 1995).
- ³⁷ A. J. Lovinger, *Science* **220**, 1115 (1983).
- ³⁸ I. Gontia, S. V. Frolov, M. Liess, E. Ehrenfreund, Z. V. Vardeny, K. Tada, H. Kajii, R. Hidayat, A. Fujii, K. Yoshino, M. Teraguchi, and T. Masuda, *Phys. Rev. Lett.* **82**, 4058 (1999).
- ³⁹ M. J. Rice and E. J. Mele, *Phys. Rev. Lett.* **49**, 1455 (1982).
- ⁴⁰ A. Geim and I. Grigorieva, *Nature* **499**, 419 (2013).
- ⁴¹ L. Britnell, R. M. Ribeiro, A. Eckmann, R. Jalil, B. D. Belle, A. Mishchenko, Y.-J. Kim, R. V. Gorbachev, T. Georgiou, S. V. Morozov, A. N. Grigorenko, A. K. Geim, C. Casiraghi, A. H. C. Neto, and K. S. Novoselov, *Science* **340**, 1311 (2013).
- ⁴² W. J. Yu, Y. Liu, H. Zhou, A. Yin, Z. Li, Y. Huang, and X. Duan, *Nature nanotechnology* **8**, 952 (2013).
- ⁴³ M. Buscema, D. J. Groenendijk, G. A. Steele, H. S. van der Zant, and A. Castellanos-Gomez, *Nature communications* **5** (2014).
- ⁴⁴ A. K. Singh and R. G. Hennig, *Applied Physics Letters* **105**, 042103 (2014).
- ⁴⁵ L. C. Gomes and A. Carvalho, *arXiv preprint arXiv:1504.05627* (2015).
- ⁴⁶ P. D. Antunez, J. J. Buckley, and R. L. Brutchey, *Nanoscale* **3**, 2399 (2011).
- ⁴⁷ L. Li, Z. Chen, Y. Hu, X. Wang, T. Zhang, W. Chen, and Q. Wang, *Journal of the American Chemical Society* **135**, 1213 (2013).
- ⁴⁸ S. Banerjee, R. Singh, V. Pardo, and W. Pickett, *Physical review letters* **103**, 016402 (2009).
- ⁴⁹ W. P. Su, J. R. Schrieffer, and A. J. Heeger, *Phys. Rev. Lett.* **42**, 1698 (1979).
- ⁵⁰ F. Xia, H. Wang, and Y. Jia, *Nature communications* **5** (2014).
- ⁵¹ E. Liu, Y. Fu, Y. Wang, Y. Feng, H. Liu, X. Wan, W. Zhou, B. Wang, L. Shao, C.-H. Ho, *et al.*, *Nature communications* **6** (2015).
- ⁵² A. N. Rudenko and M. I. Katsnelson, *Phys. Rev. B* **89**, 201408 (2014).
- ⁵³ A. Rudenko, S. Yuan, and M. Katsnelson, *arXiv:1506.01954* (2015).
- ⁵⁴ M. Ezawa, *New Journal of Physics* **16**, 115004 (2014).
- ⁵⁵ G. Montambaux, F. Piéchon, J.-N. Fuchs, and M. O. Goerbig, *Phys. Rev. B* **80**, 153412 (2009).
- ⁵⁶ M. Pagliaro, G. Palmisano, and R. Ciriminna, *Flexible solar cells* (Wiley, 2008).